Letters

Automatic Current Sharing of Paralleled Windings for *LLC* Resonant Converter With Secondary-Side Resonant Inductors

Yue Liu, Hongfei Wu, *Senior Member, IEEE*, Yunfei Wang, Guosheng Ji, and Zhengke Zhang

***Abstract*—The current sharing issue of paralleled secondary windings of the transformer is a major concern of *LLC* resonant converters. Matrix transformers solve this issue by connecting primary windings in series and secondary windings in parallel, but the volume and loss of magnetic cores increase dramatically. This letter proposes a modified *LLC* resonant converter, which can achieve automatic current sharing of secondary windings by distributing the resonant inductor to each secondary winding. Theoretical analysis indicates that the current balance of each paralleled secondary winding only depends on the inductance of distributed resonant inductors, whereas the tolerance of resonant inductors can be guaranteed easily in practice. An experimental prototype is built and tested to verify the effectiveness of the proposed method.**

***Index Terms*—Current balance, high frequency, magnetic integration, resonant converter.**

I. Introduction

LLC resonant converters have been the most popular topologies for high frequency, high efficiency, and high power density power conversion [1], [2]. Paralleled secondary windings and synchronous rectifiers (SRs) are required for low output voltage and high output current applications, such as data center, telecommunications, adapter, and consumer electronics [3]. However, current sharing of paralleled windings is a big issue impacted by many factors, such as the distance between the winding and air gap, manufacturing tolerance, termination configuration, etc., leading to significant errors between the leakage inductances and ac resistances of secondary windings [4], [5]. The current sharing issue will become more serious as the switching frequency increases. Many current sharing methods were proposed for pulsewidth modulation converters [6], [7], for example, coupled inductor is employed to achieve current sharing for forward converters, but these methods are not valid for resonant converters.

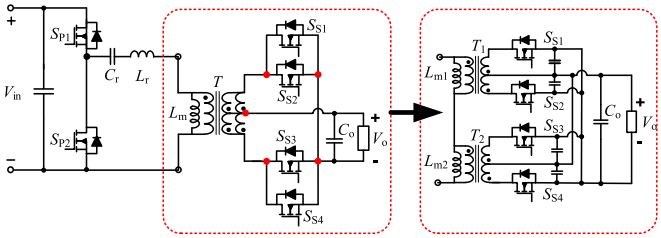

Fig. 1. Matrix transformer solutions for the *LLC* resonant converter with paralleled windings.

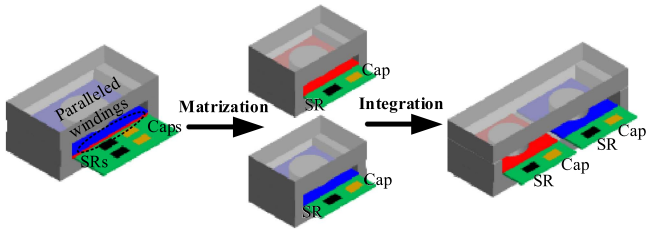

Fig. 2. Evolution process of magnetic core structures and volume for different schemes.

Recent studies have proved that a matrix transformer is an effective solution to the current sharing problems of an *LLC* resonant converter. As shown in Fig. 1, the centralized transformer is divided into several subtransformers. Current sharing of multiple secondary windings of these subtransformers is achieved automatically by connecting the primary windings of these transformers in series [8], [9]. In comparison with the centralized transformer, the total size/volume and losses of matrix transformer increases exponentially. Various magnetic integration methods for matrix transformers [10], [11], resonant inductors, and transformers [12], [13], [14] have been proposed to reduce the size/volume and improve both efficiency and power density. As shown in Fig. 2, although size/volume and loss of integrated magnetics are reduced compared to the multiple separated magnetics, the total size/volume and losses of the integrated core are still higher than the original centralized transformer. How to solve the current sharing problem of paralleled windings/SRs without sacrificing size/volume and loss of the

Manuscript received 8 June 2023; revised 1 August 2023; accepted 14 August 2023. Date of publication 21 August 2023; date of current version 22 September 2023. This work was supported in part by the National Natural Science Foundation of China under Grants 52122708 and 51977105 and in part by the Natural Science Foundation of Jiangsu Province, China, under Grant BK20200017. *(Corresponding author: Hongfei Wu.)*

The authors are with the Center for More-Electric-Aircraft Power System, College of Automation Engineering, Nanjing University of Aeronautics and Astronautics, Nanjing 211106, China (e-mail: liuyue0909@nuaa.edu.cn; wuhongfei@nuaa.edu.cn; wyf0524@nuaa.edu.cn; jiguosheng@nuaa.edu.cn; zhangzhengke@nuaa.edu.cn).

Color versions of one or more figures in this article are available at https://doi.org/10.1109/TPEL.2023.3306850.

Digital Object Identifier 10.1109/TPEL.2023.3306850

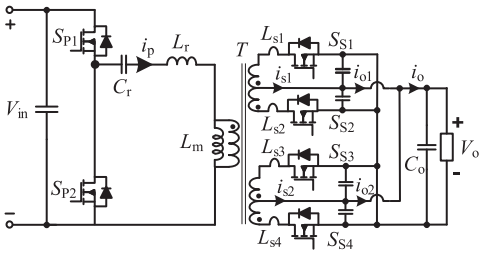

Fig. 3. *LLC* resonant converter with primary resonant inductors and centralized transformer.

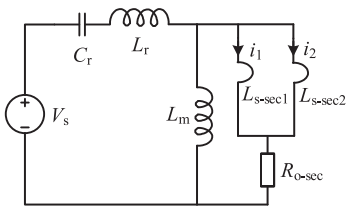

Fig. 4. Simplified equivalent circuit for the *LLC* resonant converter with primary resonant inductor.

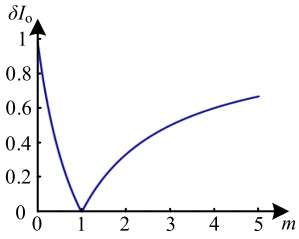

Fig. 5. Relationship between δI_o and m.

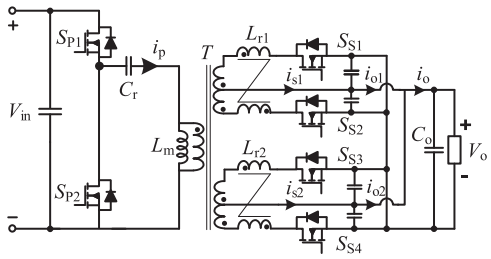

Fig. 6. Proposed *LLC* resonant converter with secondary resonant inductors and centralized transformer.

magnetic core is a problem worthy of in-depth research, which is also the major concern of this letter.

II. Theoretical Analysis of Current Sharing Performance

A. LLC *Resonant Converter With Primary Inductor and Paralleled Secondary Windings*

The topology of the *LLC* resonant converter with single primary resonant inductor and centralized transformer is shown in Fig. 3. Here, S_{P1}–S_{P2} and S_{S1}–S_{S4} are the primary and secondary switching devices. L_m, L_r, and C_r are the magnetizing inductance, primary resonant inductor, and resonant capacitor, respectively. L_{s1}–L_{s4} are the leakage inductances of four secondary windings. i_p, i_{s1}–i_{s2}, and i_{o1}–i_{o2} are the primary current, secondary ac currents, and dc currents, respectively. The simplified equivalent circuit for its resonant tank is presented in Fig. 4. As presented in the figure, V_s is the midpoint voltage of the primary leg. $L_{s\text{-}sec1}$–$L_{s\text{-}sec2}$ are the equivalent leakage inductances of two transformer secondary windings. $R_{o\text{-}sec}$ is the corresponding equivalent output resistances. i_1 and i_2 are the equivalent currents of two paralleled windings. Since their positions and terminations are different from each other, two secondary leakage inductances are usually different. Their relationship is defined as follows:

$$L_{s-\sec 2} = m \cdot L_{s-\sec 1}\,(m > 0)\,. \tag{1}$$

Since two secondary windings are paralleled, according to (1), the relationship between the current sharing error δI_o of two secondary windings (i_1 and i_2) and the leakage ratio coefficient m can be described as

$$\delta I_o = \frac{|i_1 - i_2|}{|i_1 + i_2|} = \left| \frac{\frac{1}{L_{s-\sec 1}} - \frac{1}{L_{s-\sec 2}}}{\frac{1}{L_{s-\sec 1}} + \frac{1}{L_{s-\sec 2}}} \right| = \left| \frac{\frac{L_{s-\sec 2}}{L_{s-\sec 1}} - 1}{\frac{L_{s-\sec 2}}{L_{s-\sec 1}} + 1} \right|$$

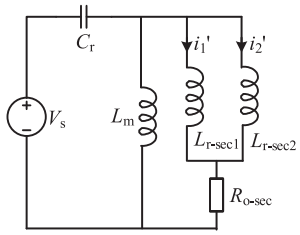

Fig. 7. Simplified equivalent circuit for the *LLC* resonant converter with two secondary resonant inductors.

$$= \left| \frac{m-1}{m+1} \right|. \tag{2}$$

As shown in Fig. 5, the relationship curve between δI_o and m is described and presented according to (2). It can be found that as the difference of the two secondary leakage inductances increases, the current sharing performance is significantly reduced. When the gap of $L_{s\text{-}sec1}$ and $L_{s\text{-}sec2}$ doubles, the current sharing error reaches 1/3. Therefore, the *LLC* resonant converter with single primary resonant inductor and centralized transformer is not suitable for paralleled secondary windings due to the poor current sharing performance.

B. LLC *Resonant Converter With Multiple Paralleled Secondary Inductors and Windings*

To improve the current sharing performance, the primary single resonant inductor is split and configured on the secondary side of the centralized transformer, as shown in Fig. 6. Therefore, the secondary leakage inductances work as part of the resonant inductors for each winding due to their direct series connection. L_{r1}–L_{r2} are the secondary-side resonant inductors, including the leakage inductances. They are decoupled from each other. Its simplified equivalent circuit is shown in Fig. 7. $L_{r\text{-}sec1}$ and

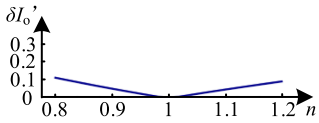

Fig. 8. Relationship between δI_o' and m'.

$L_{r\text{-}sec2}$ are the two equivalent secondary resonant inductors. i_1' and i_2' are the equivalent current of two paralleled windings with secondary inductors. Similar to the previous analysis, the relationship between $L_{r\text{-}sec1}$ and $L_{r\text{-}sec2}$ is defined as m'

$$L_{r-\sec 2} = m' \cdot L_{r-\sec 1}. \tag{3}$$

Similar to the analysis in Section II-A, according to (3), the relationship between the current sharing error δI_o' of two secondary windings (i_1' and i_2') with resonant inductors and m' can be described as

$$\delta I_o' = \frac{|i_1' - i_2'|}{|i_1' + i_2'|} = \left| \frac{\frac{1}{L_{r-sec1}} - \frac{1}{L_{r-sec2}}}{\frac{1}{L_{r-sec1}} + \frac{1}{L_{r-sec2}}} \right| = \left| \frac{\frac{L_{r-sec2}}{L_{r-sec1}} - 1}{\frac{L_{r-sec2}}{L_{r-sec1}} + 1} \right|$$
$$= \left| \frac{m' - 1}{m' + 1} \right|. \tag{4}$$

It can be easily found that (4) is a bit similar to (2). The only difference is that the secondary resonant inductors $L_{r\text{-}sec1}$–$L_{r\text{-}sec2}$ are far larger than the secondary leakage inductors $L_{s\text{-}sec1}$–$L_{s\text{-}sec2}$. Fig. 8 shows the relationships between δI_o' and m'. Since the resonant inductor is designed and controllable, their errors can be minimized by detailed processing and later adjustments. Hence, the range of m' is narrower than that of m. Obviously, the current sharing performance is greatly improved by the change of the position for resonant inductors.

III. Integrated Core Structure for the Proposed *LLC* Resonant Converter

To further reduce the volume and loss of the magnetics and thus improve the overall power density, magnetic integration is employed for the transformer and resonant inductors. Originally, three ER cores are adopted for the centralized transformer and two secondary inductors, as shown in Fig. 9(a). It should be noted that for each core, the air gap is configured only above the middle winding column. Fig. 9(b) presents the key current waveforms, including the driving voltage, primary current i_p, magnetizing current i_m, and equivalent secondary current i_s (sum of the two full-wave wingding currents). Since the magnetic flux is proportional to the current of corresponding inductor, the magnetic fluxes of the transformer and secondary resonant inductor shown in Fig. 9(c) are obtained according to the corresponding waveforms.

Due to their large flux phase difference, three magnetics can be integrated with each other according to the work in [13] and [14]. Fig. 10(a) shows the top view of the separate magnetic cores. Then, the separate magnetic plates are replaced by an integrated plate, as shown in Fig. 10(b). In addition, the magnetic columns of the resonant inductors are adjusted to crescent shape for smaller footprint. Through magnetic integration, not only the

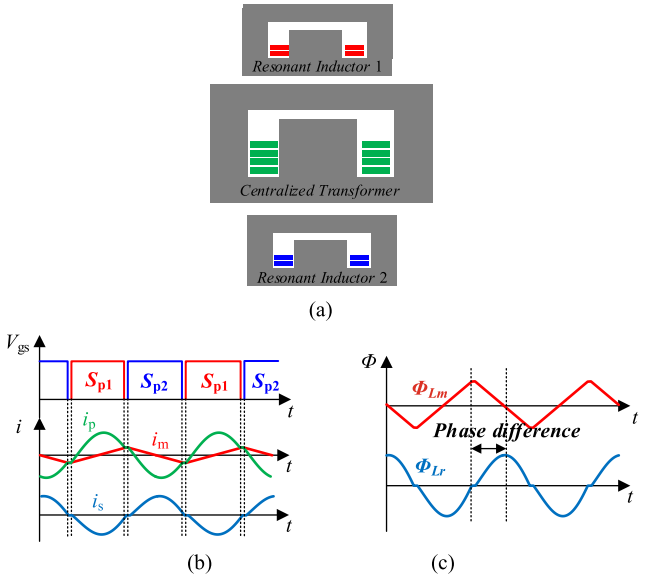

Fig. 9. Separate magnetic core structures for the transformers and resonant inductors. (a) Cross-sectional view. (b) Key current waveforms. (c) Magnetic flux phase relationship.

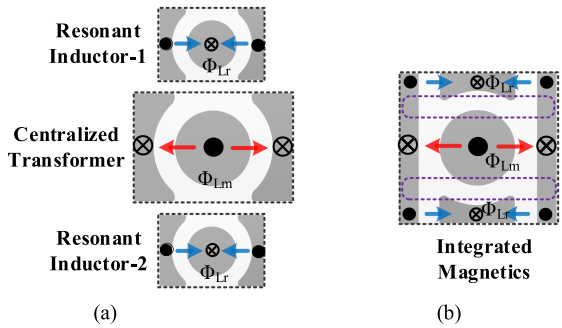

Fig. 10. Top view of magnetic core structures. (a) Separate core structures. (b) Integrated core structure.

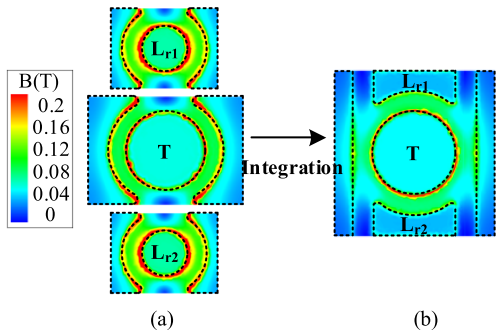

Fig. 11. Flux density comparison of different core structures. (a) Separate cores. (b) Integrated cores.

quantity of magnetics is reduced from three to one, but also the core loss and volume are decreased due to the flux cancellation marked by purple dashed box. Meanwhile, three magnetics still keep decoupled from each other. Fig. 11(a) and (b) show the comparison of the core flux density before and after magnetic integration. After integration, the flux density becomes more uniform and lower due to the increase in cross-sectional area of

TABLE I
LOSS COMPARISON BETWEEN DIFFERENT CORE STRUCTURES

	Core loss/W	Winding loss/W	Total loss/W	Volume /cm^3
Separate transformer	2.73	2.28	5.01	4.4
Separate inductors	2.24*2	0.37*2	2.61*2	1.3*2
Separate magnetics	7.21	3.02	10.23	7
Integrated magnetics	3.52(↓51%)	2.74(↓10%)	6.28(↓39%)	5.8(↓18%)

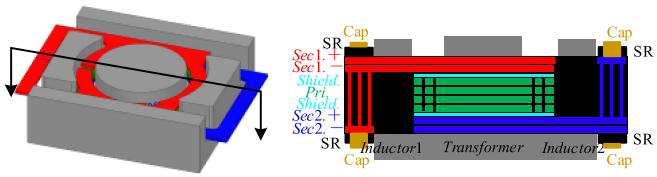

Fig. 12. Integrated core structure with "I" shape core removed. (a) 3-D view. (b) Cross-sectional view.

magnetic plates and flux cancellation. As shown in Table I, the detailed loss distribution and volume for separate magnetics and integrated magnetics are presented. Compared with the separate magnetics, both the core loss and volume are greatly reduced after integration.

Fig. 12(a) presents the 3-D view of the final integrated magnetics with "I" shape core removed. Fig. 12(b) shows the cross-sectional view of the integrate magnetics. It can be found that for the positive and negative two inductor windings of one output, they are almost full coupled. An eight-layer PCB is employed and another two shielding layers are configured between the primary and secondary windings for lower common mode noise and better electrical magnetic interference performance. Moreover, the SRs and output filter capacitors are also integrated with the secondary windings to achieve lower ac winding resistances and termination loss.

IV. SIMULATION AND EXPERIMENTAL RESULTS

A. Simulation Results

To verify the validity of the aforementioned theoretical analysis, detailed electrical simulations for various conditions are conducted. The impedance errors' influence on the current sharing performance for the *LLC* resonant converter with different inductor positions is all shown as follows.

As shown in Fig. 13(a), for the *LLC* resonant converter with primary concentrative resonant inductor, when there is a difference of about three times between two secondary equivalent leakage inductances (L_r = 14.4 μH, L_{s1}/L_{s2} = 5 nH, and L_{s3}/L_{s4} = 15 nH), the current difference between two paralleled secondary windings has almost doubled. However, for the *LLC* resonant converter with two secondary inductors, due to the controllable inductance errors, it is assumed that there exists a 10% error between two equivalent resonant inductors (L_{r1} = 0.23 μH and L_{r2} = 0.25 μH). Since the current sharing

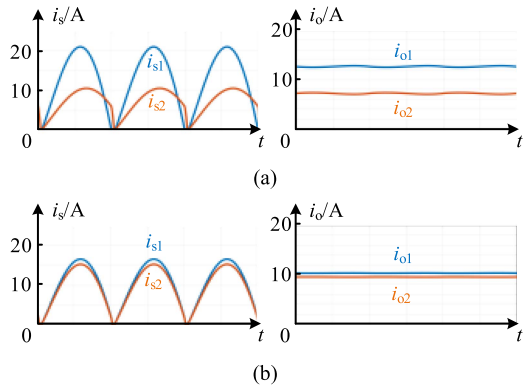

Fig. 13. Current sharing performance with different secondary inductances. (a) m = 3 (L_r = 14.4 μH, L_{s1}/L_{s2} = 5 nH, and L_{s3}/L_{s4} = 15 nH). (b) m' = 1.1. (L_{r1} = 0.23 μH and L_{r2} = 0.25 μH).

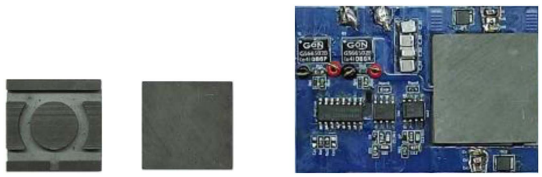

Fig. 14. 500-kHz 400-W 400-V/20-V *LLC* converter prototype. (a) Integrated magnetics. (b) Fully assembled prototype.

TABLE II
SPECIFICATIONS OF THE *LLC* RESONANT CONVERTER

	LLC with Paralleled Windings
Resonant frequency	500 kHz
Transformer turns ratio	12:1:1:1:1
Primary devices	GS66502B
Secondary devices	BSZ037N06LS5
Resonant capacitor	7 nF
Resonant inductor	0.24 μH // 0.24μH
Magnetizing inductor	86.4 μH

performance of two secondary paralleled windings depends on the paralleled inductances. The current sharing performance is greatly improved according to the simulation results shown in Fig. 13(b).

B. Experimental Results

Based on the integrated core structure and winding structure shown in Fig. 14(a), a 500-kHz, 400-V/20-V, 400-W *LLC* resonant converter prototype is built, as shown in Fig .14(b). The key parameters of the prototype are shown in Table II.

Steady experimental waveforms under full load are shown in Fig. 15. It is found that zero voltage switching can be achieved for all the primary switching devices during the full-load range. Due to the difficulty in measuring ac current in the PCB winding structure employed in this letter, two output dc currents under different loads are measured and shown in Fig. 16(a) and (b). Furthermore, more detailed dc current data for the paralleled windings are tested and shown in Table III. No matter how

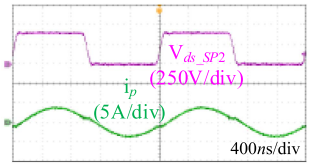

Fig. 15. Steady waveforms under full load.

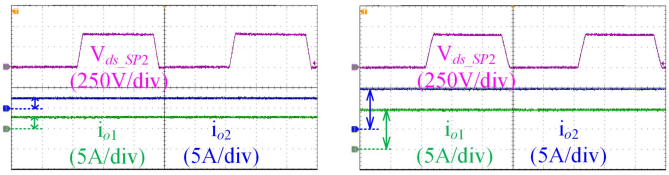

Fig. 16. Current sharing performance under different loads. (a) Under light (25%) load. (b) Under full (100%) load.

TABLE III
DC CURRENTS OF THE PROPOSED DC–DC CONVERTER

i_o/A	i_{o1}/A	i_{o2}/A
4.00	2.02	1.98
8.02	4.04	3.98
11.98	6	5.98
16.02	8.04	7.98
20.04	10.12	9.92

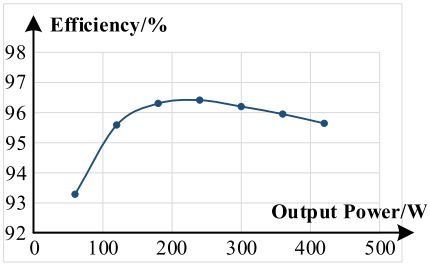

Fig. 17. Test efficiency.

heavy the load is, excellent current sharing performance can be obtained between two outputs, which is consistent with the theoretical analysis. Finally, the efficiency of the *LLC* resonant converter with paralleled windings is tested and shown in Fig. 17. As the demo prototype in this letter is mainly built for testing the current sharing performance conveniently, its power loop and efficiency have not been optimized for design. Hence, there is still some room for the efficiency improvement, which is also one of the future works.

V. CONCLUSION

This letter proposed a modified *LLC* resonant converter with paralleled secondary resonant inductors, which can achieve automatic current sharing. Since the current sharing performance depends on the paralleled inductances' errors. By splitting the single resonant inductor into multiple secondary inductors, which are designed and controllable, the paralleled inductance errors can be minimized. In this way, more secondary windings can be directly connected in parallel for higher current output applications. Also, an integrated magnetic core structure is proposed for the transformer and two secondary resonant inductors. A 400-W *LLC* resonant converter with two paralleled secondary windings was built. Both simulation and experimental results under different conditions verify the effectiveness of the proposed scheme.

ACKNOWLEDGMENT

The authors would like to thank Hengdian Group Dongci Company, Ltd., for providing high-frequency magnetic cores for the research in this letter.

REFERENCES

[1] Y. Wei, Q. Luo, and A. Mantooth, "Overview of modulation strategies for LLC resonant converter," *IEEE Trans. Power Electron.*, vol. 35, no. 10, pp. 10423–10443, Oct. 2020.
[2] L. A. D. Ta, N. D. Dao, and D.-C. Lee, "High-efficiency hybrid LLC resonant converter for on-board chargers of plug-in electric vehicles," *IEEE Trans. Power Electron.*, vol. 35, no. 8, pp. 8324–8334, Aug. 2020.
[3] C. Liu et al., "Magnetic-coupling current-balancing cells based input-parallel output-parallel LLC resonant converter modules for high-frequency isolation of DC distribution systems," *IEEE Trans. Power Electron.*, vol. 31, no. 10, pp. 6968–6979, Oct. 2016.
[4] Y. Liu, Y. Song, D. Hu, Y. Li, Z. Zhang, and H. Wu, "Overview of planar magnetics for high-frequency resonant converters," *Chin. J. Elect. Eng.*, vol. 8, no. 4, pp. 61–78, Dec. 2022.
[5] Q. Ma, Q. Huang, and A. Q. Huang, "Performance analysis of an input-series-output-parallel LLC resonant converter with parameters mismatch," in *Proc. IEEE Energy Convers. Congr. Expo.*, Vancouver, BC, Canada, 2021, pp. 3203–3210.
[6] N. Barry and B. Daly, "Coupled magnetic amplifiers in forward converter topologies," *IEEE Trans. Power Electron.*, vol. 14, no. 1, pp. 168–176, Jan. 1999.
[7] K. I. Hwu and S.-C. Chou, "A simple current-balancing converter for LED lighting," in *Proc. 24th Annu. IEEE Appl. Power Electron. Conf. Expo.*, Washington, DC, USA, 2009, pp. 587–590.
[8] D. Huang, S. Ji, and F. C. Lee, "Matrix transformer for LLC resonant converters," in *Proc. 28th Annu. IEEE Appl. Power Electron. Conf. Expo.*, Long Beach, CA, USA, 2013, pp. 2078–2083.
[9] D. Huang, S. Ji, and F. C. Lee, "LLC resonant converter with matrix transformer," *IEEE Trans. Power Electron.*, vol. 29, no. 8, pp. 4339–4347, Aug. 2014.
[10] C. Fei, F. C. Lee, and Q. Li, "High-efficiency high-power-density LLC converter with an integrated planar matrix transformer for high-output current applications," *IEEE Trans. Ind. Electron.*, vol. 64, no. 11, pp. 9072–9082, Nov. 2017.
[11] A. Nabih, R. Gadelrab, P. R. Prakash, Q. Li, and F. C. Lee, "High power density 1 MHz 3 kW 400 V-48 V LLC converter for datacenters with improved core loss and termination loss," in *Proc. IEEE Appl. Power Electron. Conf. Expo.*, 2021, pp. 304–309.
[12] M. H. Ahmed, A. Nabih, F. C. Lee, and Q. Li, "Low-loss integrated inductor and transformer structure and application in regulated LLC converter for 48-V bus converter," *IEEE J. Emerg. Sel. Topics Power Electron.*, vol. 8, no. 1, pp. 589–600, Mar. 2020.
[13] Y. Liu, H. Wu, J. Zou, Y. Tai, and Z. Ge, "CLL resonant converter with secondary side resonant inductor and integrated magnetics," *IEEE Trans. Power Electron.*, vol. 36, no. 10, pp. 11316–11325, Oct. 2021.
[14] Y. Liu, H. Wu, Z. Ge, and G. Ji, "Magnetic integration for multiple resonant converters," *IEEE Trans. Ind. Electron.*, vol. 70, no. 8, pp. 7604–7614, Aug. 2023.